The effect of electronic excitation on London dispersion

Xibo Feng,[1] Alberto Otero-de-la-Roza,[2] and Erin R. Johnson[1, a)]

[1)] *Department of Chemistry, Dalhousie University, 6274 Coburg Rd, P.O.Box 15000 B3H 4R2, Halifax, Nova Scotia, Canada*

[2)] *Department of Chemistry, University of British Columbia, Okanagan, 3247 University Way, Kelowna, British Columbia, Canada V1V 1V7.*

(Dated: 12 January 2018)

[a)] Electronic mail: erin.johnson@dal.ca; Telephone: 902-494-3409

Abstract

Atomic and molecular dispersion coefficients can now be calculated routinely using density-functional theory. In this work, we present the first determination of how electronic excitation affects molecular C_6 London dispersion coefficients from the exchange-hole dipole moment (XDM) dispersion model. Excited states are typically found to have larger dispersion coefficients than the corresponding ground states, due to their more diffuse electron densities. A particular focus is both intramolecular and intermolecular charge-transfer excitations, which have high absorbance intensities and are important in organic dyes, light-emitting diodes, and photovoltaics. In these classes of molecules, the increase in C_6 for the electron-accepting moiety is largely offset by a decrease in C_6 for the electron-donating moiety. As result, the change in dispersion energy for a chromophore interacting with neighbouring molecules in the condensed phase is minimal.

Keywords: London dispersion, excited states, density-functional theory

I. INTRODUCTION

The study of electronic excitations is essential in many areas of chemistry. Molecular electronic excitations play important roles in the design and fabrication of organic electronics[1,2] (sensors, light-emitting diodes, photovoltaics, etc.). While properties of the excited state have been extensively studied for single molecules in the gas-phase and in solution, little is known regarding how excitation of a single molecule affects the intermolecular interactions with its neighbours.[3,4] In particular, to our knowledge, there has only been one investigation to date as to how electronic excitation affects the strength of intermolecular London dispersion interactions[5] and this was limited to a small set of van der Waals complexes rather than common chromophores.[6] This may be, in part, because popular empirical dispersion models have dispersion coefficients that are either fixed[7] or depend only on the geometry[8] and consequently cannot describe correctly the change in intermolecular dispersion during a vertical excitation. Alternatively, while non-local density-functional dispersion models are transferable to excited states,[5] they do not directly provide atomic or molecular dispersion coefficients.

The exchange-hole dipole moment (XDM) model[9–11] in the context of density-functional theory (DFT) is uniquely suited to address the question of how electronic excitation affects London dispersion. The XDM model provides a non-empirical means of calculating accurate C_6 (and higher-order[12]) dispersion coefficients directly from the electron density. As such, the XDM dispersion coefficients are sensitive to changes in an atom's electronic environment[13–15] and the method is completely transferable, without modification, from ground-state to excited-state electron densities.

In XDM, the dispersion energy is an *a posteriori* correction to the self-consistent energy, calculated using one of the common density functionals. The dispersion energy is written as a sum over all pairs of atoms, i and j separated by a distance R_{ij}, and includes C_6, C_8, and C_{10} dispersion terms.

$$E_{\text{disp}}^{\text{XDM}} = -\sum_{n=6,8,10}\sum_{i<j}\frac{C_{n,ij}f_n(R_{ij})}{R_{ij}^n} \tag{1}$$

The damping function, $f_n(R_{ij})$, prevents the divergence of the dispersion energy at small internuclear separations. The atomic C_6 dispersion coefficients are determined from the

exchange-hole dipole moment integrals, $\langle d_X^2 \rangle$, and atom-in-molecule polarisabilities, α.

$$C_{6,ij} = \frac{\alpha_i \alpha_j \langle d_X^2 \rangle_i \langle d_X^2 \rangle_j}{\alpha_i \langle d_X^2 \rangle_j + \alpha_j \langle d_X^2 \rangle_i} \tag{2}$$

Analogous formulae can be written for the higher-order dispersion coefficients and involve higher-order exchange-hole multipole moments. The moment integrals and polarisabilities are both functions of the electron density and consequently vary with atomic environment. Interested readers are directed to Ref. 11 for a comprehensive review of the XDM equations and the theory underpinning the model. The overall molecular C_n dispersion coefficient can be evaluated by summing over all atom pairs.

$$C_n = \sum_{ij} C_{n,ij} \tag{3}$$

This value is the C_n dispersion coefficient for the interaction between one molecule and a second, identical molecule.

In this work, the XDM model is applied to investigate how the molecular dispersion coefficients change upon electronic excitation for a small collection of molecular systems, which can be broken down into three classes. These are $\pi \rightarrow \pi^*$ excitations in conjugated hydrocarbons, charge-transfer excitations in push-pull chromophores of 4,4′-disubstituted biphenyls, and intermolecular excitations in charge-transfer complexes. Additionally, we consider a set of ten molecular crystals and co-crystals and assess how changes in dispersion coefficients resulting from electronic excitation affect the dispersion energy for interaction of a single, excited molecule with the surrounding bulk. This dispersion contribution to the excitation energy has not previously been considered when modeling electronic excitations of molecules in the condensed phase.

II. COMPUTATIONAL METHODS

A. Molecular calculations

All molecular calculations were performed using the Gaussian 09 program.[16] Geometries of all molecules and intermolecular complexes were optimized using B3LYP[17,18] or B3LYP-XDM, respectively, both with the 6-31+G* basis set. Subsequent single-point en-

ergy calculations and time-dependent density-functional theory (TD-DFT)[19–22] calculations were performed with either the 6-31+G* basis set for single molecules or aug-cc-pVDZ for complexes and either the B3LYP[17,18] or CAM-B3LYP[23] density functionals. Usually the first singlet excited state was considered, but occasionally the density was determined for a higher excited state corresponding to the charge-transfer state for the push-pull chromophores or intermolecular charge-transfer complexes (see below).

Change-transfer excitations are well known to be problematic for functionals with little or no exact-exchange mixing,[24–30] due to the density-functional "delocalisation" or "charge-transfer" error.[31–36] As such, calculations on intermolecular charge-transfer complexes were performed using systematic series of hybrid and range-separated hybrid density functionals with varying exact-exchange mixing. Specifically, a family of BLYP[18,37]-based hybrid functionals of the form

$$E_{\mathrm{XC}} = a_{\mathrm{X}} E_X^{\mathrm{exact}} + (1 - a_{\mathrm{X}}) E_{\mathrm{X}}^{\mathrm{B88}} + E_{\mathrm{C}}^{\mathrm{LYP}} \tag{4}$$

was used, where the exact-exchange mixing fraction, a_{X} was varied from 0 to 1 in increments of 0.1. Similarly, we also considered a family of range-separated hybrid functionals based on LC-BLYP.[38] In these functionals, the interelectronic Coulomb potential is divided into short- and long-range terms using the error function:

$$\frac{1}{r_{12}} = \frac{1 - \mathrm{erf}(\omega r_{12})}{r_{12}} + \frac{\mathrm{erf}(\omega r_{12})}{r_{12}}. \tag{5}$$

This modified Coulomb potential is then used in evaluation of the exchange energy such that the short-range portion is treated with the B88 generalised-gradient-approximation functional[37] and the long-range component is treated with exact exchange. The length of this range-separation is determined by the parameter ω, whose value was varied from 0 to 1 Bohr^{-1} in increments of 0.1 Bohr^{-1}.

In evaluation of the exchange-hole dipole moments, and resulting XDM dispersion coefficients, the Becke-Roussel exchange-hole model[39] was used in all calculations. As such, the full two-particle density matrix for the excited state was not required. We need only the expansion of the Kohn-Sham orbitals in terms of the atomic basis functions, which can be obtained from the wavefunction file. The "density=current" option in the Gaussian

program[16] was used to generate wavefunction files for excited states. The ground state density, ρ_{gs}, is obtained from the usual sum of the squares of the occupied, real Kohn-Sham orbitals: $\rho_{gs} = \sum_{i,\sigma} \psi_{i\sigma}^2(\boldsymbol{r})$. The excited-state density, ρ_{ex} is determined from the first-order density response and is given by[40,41]

$$\rho_{ex} = \rho_{gs} + \sum_{i,a,\sigma} P_{ia\sigma}\psi_{i\sigma}(\boldsymbol{r})\psi_{a\sigma}(\boldsymbol{r}), \tag{6}$$

where index i refers to the occupied Kohn-Sham orbitals, index a the virtual Kohn-Sham orbitals, and σ denotes the electron spin. The $P_{ia\sigma}$ coefficients are determined from solution of the Casida equation in TD-DFT.[19,42] The usual BR procedure is then applied to calculate the exchange-hole dipole moments and dispersion coefficients[10,11,43] from the density and orbitals. The postg program[44] was used to calculate the C_6 dispersion coefficients and Hirshfeld[45] atomic charges for both the ground and excited states.

B. Solid-state calculations

Crystal structures of 4-amino-4′-nitrobiphenyl, A3MN [2-Amino-3-((E)-(4-(diethylamino) benzylidene)amino)maleonitrile],[46] coumarin, 6-aminocoumarin, and the benzene/hexafluorobenzene, N,N-dimethylaniline/hexafluorobenzene, naphthalene/hexafluorobenzene, tetracyanoethylene/naphthalene, chloranilic acid/pyrazine, and 2,5-dimethylbenzoquinone/bis-(hydroquinone) co-crystals, were obtained from the Cambridge Crystallographic Data Centre[47] (codes: KEFLEM01, PAQMIE01, RAZLEK, BEZZAJ, BICVUE01, DMAFBZ01, IVOBOK, CYENAP, BOQHOE, and CISCOW, respectively). The structures of these crystals (both atomic positions and unit-cell parameters) were then optimized with B86bPBE-XDM[11,48–50] using the Quantum ESPRESSO program.[51] These calculations used Projector-Augmented-Wave (PAW) pseudopotentials, a $4\times4\times4$ k-point mesh, and energy and density plane-wave cut-offs of 60 and 600 Ry, respectively. After optimization, single-point energy and TD-DFT calculations were performed on a single molecule cut from the crystal at this fixed geometry. These calculations used Gaussian 09 as detailed above, with the B3LYP functional and the 6-31+G* basis set. The London dispersion coefficients were calculated from the resulting electron densities using the postg program.[44] These coefficients were then used to evaluate the dispersion energy for interaction of this single molecule, in either its

ground or excited state, with the remainder of the crystal, using the critic2 program.[52]

III. RESULTS AND DISCUSSION

A. Conjugated hydrocarbons

We begin by considering the $\pi \rightarrow \pi^*$ excitations for the set of conjugated hydrocarbon molecules shown in Figure 1. This set consists of a mixture of straight-chain alkenes, biphenyls, and stilbenes. As $\pi \rightarrow \pi^*$ excitations are much less sensitive to the choice of DFT method than are charge-transfer excitations, we consider only B3LYP results. Figure 2 shows the percent change in molecular C_6 dispersion coefficients for all members of this set, as a function of either excitation energy (a,b) or chain length (c,d).

The results in Figure 2(a,b) show that the percent change in molecular C_6 upon excitation increases exponentially with increasing excitation energy for each distinct series of compounds (alkenes, stilbenes, and biphenyls). This is to be expected as the valence electron becomes more weakly bound in higher-energy excited states, causing the electron density to be more diffuse, which in turn causes the dispersion coefficients to increase. In particular the percent increase in C_6 upon excitation of ethylene is extremely large (in excess of 200%) and even larger increases appear in high-energy Rydberg excitations. However, as such high-energy excitations are not observed in everyday chemical applications, we focus our attention on lower-energy $\pi \rightarrow \pi^*$ and charge-transfer excitations.

While the excitation energies for the conjugated-chain set vary significantly depending on the molecule type, a simplified picture of the effect of excitation on C_6 can be obtained by recourse to a particle-in-a-box model in which only the chain length of each hydrocarbon is considered. Figure 2(c,d) shows the that percent change in C_6 decreases with increasing chain length, using two possible definitions (either the Euclidean length or number of C-C bonds between distal carbon atoms, with the latter yielding a slightly improved correlation). In the context of the particle-in-a-box, a shorter chain, or box, length results in a more loosely-bound excited state, leading to large increases in C_6 upon excitation. Conversely, a longer chain length results in a more-tightly bound excited state, leading to smaller relative increases in C_6 upon excitation. Figure 2(c,d) also shows that C_8 and C_{10} follow the same trends as seen for C_6, although the percentage increase induced by the excitation is higher

for the higher-order dispersion coefficients.

Lastly, we decompose the changes in C_6 into contributions from the two types of terms in Equation 2: the moment integrals and atomic polarisabilities. As the densities in the excited states are more diffuse, one might expect that an increase in polarisability would be the primary contribution to the change in molecular C_6. However, more diffuse densities will also cause a larger average displacement between a reference electron and its corresponding exchange hole, which remains centered near the nearest atomic nucleus.[39] Thus the moment integrals also increase upon excitation, and Figure 3 shows that the relative contributions from the moment integrals and polarisabilities are roughly equivalent. This is similar to what is seen for changing chemical environments in ground-state molecules,[11,13] but contrary to solids where changes in C_6 are dominated by changes in the exchange-hole dipole moment integrals.[11,14]

B. Push-pull chromophores

Next we consider the set of 4,4'-disubstituted biphenyls shown in Figure 4(a). These molecules can be classified as "push-pull" systems since one substituent is a strong electron-donating group (EDG) while the other is an electron-withdrawing group (EWG). In all cases either the first or second excited state corresponds to a charge-transfer state, as determined from the Hirshfeld charges. In our analysis, the charges and dispersion coefficients of these molecules are partitioned into contributions from the electron-donating and electron-accepting halves which are separated by the central C-C single bond. The extent of charge transfer is determined as the absolute value of the difference in the Hirshfeld charge between the ground and excited state, for either of these two halves of a given molecule.

Figure 4(b) shows the extent of charge transfer as a function of the calculated excitation, with both B3LYP and CAM-B3LYP. Range-separated functionals, such as CAM-B3LYP, are conventionally viewed as being the more reliable for charge-transfer excitations,[53–56] although one must be careful not to generalise this result, particularly to large systems, as the performance of range-separated functionals is highly system-dependent.[57–59] Figure 4(b) shows that going from B3LYP to CAM-B3LYP leads to higher excitation energies and reduced charge transfer, as expected since the latter functional was designed to minimise charge-transfer errors. However, the correlation between these two quantities becomes less

clear than with B3LYP. Considering trends with substituent, the amino group is a stronger EDG than the hydroxyl group, resulting in greater charge-transfer and lower excitation energies. For the EWGs, the excitation energies follow the trend $NO_2 < CHO < COOH < CN < CF_3$ and the extent of charge transfer follows the inverse trend.

Figure 4 also shows the change in C_6 for the EDG and EWG halves of the biphenyls, obtained with B3LYP (c) and CAM-B3LYP (d). In general, the C_6 for the EDG decreases upon excitation as charge is transferred away from this region of the molecule, resulting in a more compact electron density. Conversely, the C_6 for the EWG increases upon excitation as charge is transferred to this region of the molecule, resulting in a more diffuse electron density. CAM-B3LYP predicts somewhat lower charge transfer, which results in smaller increases in the EWG C_6 and smaller decreases in the EDG C_6 compared to B3LYP. However, as these effects offset, the overall differences in total C_6 values remain small and are only 0-4% for the molecules in the set, with both functionals.

Lastly, regarding substituent effects, the magnitude of ΔC_6 for the EDG tends to increase with greater charge transfer, as it becomes more positive in the excited state. For the EWG, the ΔC_6 tends to increase as the extent of charge transfer decreases. This is due to the inverse relationship between charge transfer and excitation energy; reduced charge transfer occurs when the excited state is higher in energy, resulting in more diffuse electron densities and higher C_6 coefficients in the excited state. Additionally, two distinct trends lines are present in Figure 4(c,d), one for each EDG, with larger increases in C_6 occurring for the amino substituent than for the hydroxyl substituent.

C. Intermolecular charge-transfer excitations

As shown in the previous section, overall increases in molecular dispersion coefficients on excitation are minimal for intramolecular charge-transfer excitations. In this section, we consider two intermolecular charge-transfer complexes: benzene/hexafluorobenzene (in C_{6v} symmetry) and benzene/tetracyanoethylene (in C_{2v} symmetry), both of which possess fairly low-lying intermolecular charge-transfer excitations. Due to the delocalisation (or charge-transfer) error, we expect the results for these intermolecular complexes to be much more sensitive to the choice of density functional than were the data for the biphenyls. We therefore consider the effect of exact-exchange mixing on the extent of excitation-induced

charge transfer and changes in the C_6 coefficients using series of hybrid and range-separated hybrid functionals.

Figure 5(a,b) show plots of the charge-transfer excitation energy as a function of exact-exchange mixing fraction or range-separation parameter for the two intermolecular complexes. In general, the density-functional delocalisation error causes local density functionals (i.e. those with no exact-exchange mixing) to over-stabilise fractional charges and to underestimate charge-transfer excitation energies[24–36]. This is reflected in Figure 5(a,b) which show systematic increases in the excitation energies as the exact-exchange mixing fraction or range-separation parameter is increased.

Next, Figure 5(c,d) show the excitation-induced charge transfer and reveal differing behaviour for these complexes. In both cases, the BLYP functional, with no exact-exchange mixing, predicts fractional charge transfer of near one-half of an electron (0.58 e^- for benzene/hexafluorobenzene and 0.44 e^- for benzene/tetracyanoethylene). This is expected as delocalisation error causes local functionals to over-stabilise fractional charges. As exact exchange is incorporated into the functional, the extent of charge transfer tends towards integer values. However, the tends are opposing for the complexes, with the charge transfer decreasing to zero for benzene/hexafluorobenzene and increasing to 0.8 e^- for benzene/tetracyanoethylene. This would seem to imply that the latter case is a "true" charge-transfer excitation, while the low-energy charge-transfer excitation seen in the former complex is an artifact caused by delocalisation error.

Finally, Figure 5(e,f) show the excitation-induced changes in C_6 London dispersion coefficients for the complexes, as well as for the component donor and acceptor molecules. Despite the high sensitivity of both the charges and excitation energies, the dispersion coefficients show minimal functional dependence, particularly for benzene/tetracyanoethylene. This indicates that use of popular hybrid functionals, like B3LYP, should be adequate to describe dispersion properties, even for strong charge-transfer excitations. As for the disubstituted biphenyls, the C_6 of the electron donor decreases on excitation while the C_6 of the electron acceptor increases. These effects offset almost completely for benzene/tetracyanoethylene; however, for benzene/hexafluorobenzene, there is a net increase in C_6 of roughly 10%, much larger than those seen in the biphenyls or conjugated hydrocarbons. This implies that changes in dispersion energy coming from excitation may be much larger for co-crystals than single-molecule crystals, and this will be confirmed in the following section.

D. Dispersion in crystalline solids

Having established that electronic excitation has the potential to cause large changes in molecular dispersion coefficients, we next assess the impact of this effect on the dispersion energy for interaction of a single molecule with a surrounding crystal environment. We consider a set of 4 single-molecule crystals and 6 co-crystals, shown in Figure 6.

The results in Table I show that the changes in C_6 on excitation remain quite low for the single molecules exhibiting intramolecular charge-transfer excitations, as expected from the results in Section III B. While $\%\Delta C_6$ may be significantly larger in magnitude for some of the intermolecular charge-transfer excitations, the resulting changes in dispersion energy for excitation of a molecular dimer within the co-crystal remain quite small in magnitude. This is partly because the moment integrals and polarisabilities for only a single molecular dimer are changing, so the resulting effect on the dispersion coefficients for interactions with the remainder of the crystal are effectively halved relative to what would be seen for interaction between two excited moieties. Additionally, the larger relative increases in the higher-order dispersion coefficients (Figure 1) cause increases in the effective atomic van der Waals radii used in the XDM damping function. This results in increased damping of the dispersion energy, which largely offsets the effect of increasing dispersion coefficients. Indeed, in the majority of cases considered, the increased damping causes a lower dispersion energy in the excited state than in the ground state, as reflected by the many positive values of ΔE_{disp} in Table I.

The largest changes in dispersion energy resulting from a localised excitation are -1.2 kcal/mol for benzene/hexafluorobenzene and 1.2 kcal/mol for naphthalene/hexafluorobenzene. While examples could likely be found with larger dispersion-energy changes, this finding indicates that this dispersion effect has a very minor contribution to the overall excitation energy for a molecule or dimer in the condensed phase.

IV. SUMMARY

This is the first work to consider the effect of electronic excitation on molecular London dispersion coefficients. Excitation increases the dispersion coefficients as the electron density distribution in the excited state is more diffuse, resulting in larger atomic polarisabilities

and exchange-hole multipole moment integrals, with these two contributions being roughly equivalent in size. The percentage change in the C_6 dispersion coefficient was found to decrease with increasing chain length for $\pi \rightarrow \pi^*$ excitations in conjugated hydrocarbons. For charge-transfer excitations, the dispersion coefficients for the electron-donating moiety decrease, while the dispersion coefficients for the electron-withdrawing moiety increase. The combined effect on the overall dispersion coefficient is negligible for intramolecular charge transfer, but can be fairly large for intermolecular charge transfer. However, despite the potential for large changes in dispersion coefficients, electronic excitation of a single molecule has only a minimal effect on the dispersion energy for interaction of the chromophore with the surrounding bulk in a molecular crystal or co-crystal.

V. ACKNOWLEDGEMENTS

The authors thank the Natural Sciences and Engineering Research Council of Canada (NSERC) for financial support (E.R.J.) and Compute Canada (ACEnet and Westgrid), for computational time. We also thank Dr. Stephen G. Dale for helpful discussions.

REFERENCES

[1]Y. Yang, B. Rice, X. Shi, J. R. Brandt, R. Correa da Costa, G. J. Hedley, D.-M. Smilgies, J. M. Frost, I. D. W. Samuel, A. Otero-de-la-Roza, E. R. Johnson, K. E. Jelfs, J. Nelson, A. J. Campbell, and M. J. Fuchter, ACS Nano **11**, 8329 (2017).

[2]M. K. Ravva, A. Risko, and J.-L. Brédas, in *Non-covalent Interactions in Quantum Chemistry and Physics*, edited by A. Otero-de-la Roza and G. A. DiLabio (Elsevier, 2017) Chap. 9, pp. 277–302.

[3]W. Barford, N. Paiboonvorachat, and D. Yaron, J. Chem. Phys. **134**, 234101 (2011).

[4]C. Amovilli and F. M. Floris, J. Phys. Chem. A **119**, 5327 (2015).

[5]Y. Ikabata and H. Nakai, J. Chem. Phys. **137**, 124106 (2012).

[6]A. D. Laurent, C. Adamo, and D. Jacquemin, Phys. Chem. Chem. Phys **16**, 14334 (2014).

[7]S. Grimme, J. Comput. Chem. **27**, 1787 (2006).

[8]S. Grimme, J. Antony, S. Ehrlich, and H. Krieg, J. Chem. Phys. **132**, 154104 (2010).

[9]A. D. Becke and E. R. Johnson, J. Chem. Phys. **127**, 154108 (2007).

[10]A. Otero-de-la Roza and E. R. Johnson, J. Chem. Phys. **138**, 204109 (2013).

[11]E. R. Johnson, in *Non-covalent Interactions in Quantum Chemistry and Physics*, edited by A. Otero-de-la Roza and G. A. DiLabio (Elsevier, 2017) Chap. 5, pp. 169–194.

[12]A. Otero-de-la Roza and E. R. Johnson, J. Chem. Phys. **138**, 054103 (2013).

[13]E. R. Johnson, J. Chem. Phys. **135**, 234109 (2011).

[14]M. S. Christian, A. Otero-de-la-Roza, and E. R. Johnson, J. Chem. Theory. Comput. **12**, 3305 (2016).

[15]M. Mohebifar, E. R. Johnson, and C. N. Rowley, J. Chem. Theory Comput. (2017), submitted.

[16]M. J. Frisch, G. W. Trucks, H. B. Schlegel, G. E. Scuseria, M. A. Robb, J. R. Cheeseman, G. Scalmani, V. Barone, B. Mennucci, G. A. Petersson, H. Nakatsuji, M. Caricato, X. Li, H. P. Hratchian, A. F. Izmaylov, J. Bloino, G. Zheng, J. L. Sonnenberg, M. Hada, M. Ehara, K. Toyota, R. Fukuda, J. Hasegawa, M. Ishida, T. Nakajima, Y. Honda, O. Kitao, H. Nakai, T. Vreven, J. A. Montgomery, Jr., J. E. Peralta, F. Ogliaro, M. Bearpark, J. J. Heyd, E. Brothers, K. N. Kudin, V. N. Staroverov, R. Kobayashi, J. Normand, K. Raghavachari, A. Rendell, J. C. Burant, S. S. Iyengar, J. Tomasi, M. Cossi, N. Rega, J. M. Millam, M. Klene, J. E. Knox, J. B. Cross, V. Bakken, C. Adamo, J. Jaramillo, R. Gomperts, R. E. Stratmann, O. Yazyev, A. J. Austin, R. Cammi, C. Pomelli, J. W. Ochterski, R. L. Martin, K. Morokuma, V. G. Zakrzewski, G. A. Voth, P. Salvador, J. J. Dannenberg, S. Dapprich, A. D. Daniels, O. Farkas, J. B. Foresman, J. V. Ortiz, J. Cioslowski, and D. J. Fox, "Gaussian 09 Revision A.1," Gaussian Inc. Wallingford CT 2009.

[17]A. D. Becke, J. Chem. Phys. **98**, 5648 (1993).

[18]C. Lee, W. Yang, and R. G. Parr, Phys. Rev. B **37**, 785 (1988).

[19]M. E. Casida, in *Recent Advances in Density Functional Methods, Vol 1*, edited by D. P. Chong (World Scientific, Singapore, 1995) Chap. 5, pp. 155–192.

[20]R. Bauernschmitt and R. Ahlrichs, Chem. Phys. Lett. **256**, 454 (1996).

[21]R. E. Stratmann, G. E. Scuseria, and M. J. Frisch, J. Chem. Phys. **109**, 8218 (1998).

[22]C. Adamo and D. Jacquemin, Chem. Soc. Rev. **42**, 845 (2013).

[23]T. Yanai, D. P. Tew, and N. C. Handy, Chem. Phys. Lett. **393**, 51 (2004).

[24]D. J. Tozer, R. D. Amos, N. C. Handy, B. O. Roos, and L. Serrano-Andrès, Mol. Phys. **97**, 859 (1999).

[25]Z.-L. Cai, K. Sendt, and J. R. Reimers, J. Chem. Phys. **117**, 5543 (2002).

[26]A. Dreuw, J. L. Weisman, and M. Head-Gordon, J. Chem. Phys. **119**, 2943 (2003).

[27]D. J. Tozer, J. Chem. Phys. **119**, 12697 (2003).

[28]O. Gritsenko and E. J. Jan Baerends, J. Chem. Phys. **121**, 655 (2004).

[29]G. Sini, J. S. Sears, and J.-L. Bredas, J. Chem. Theory Comput. **7**, 602 (2011).

[30]S. N. Steinmann, C. Piemontesi, A. Delacht, and C. Corminboeuf, J. Chem. Theory Comput. **8**, 1629 (2012).

[31]E. Ruiz, D. R. Salahub, and A. Vela, J. Phys. Chem. **100**, 12265 (1996).

[32]A. Ruzsinszky, J. P. Perdew, G. I. Csonka, O. A. Vydrov, and G. E. Scuseria, J. Chem. Phys. **125**, 194112 (2006).

[33]A. J. Cohen, P. Mori-Sánchez, and W. Yang, Science **321**, 792 (2008).

[34]M.-C. Kim, E. Sim, and K. Burke, Phys. Rev. Lett. **111**, 073003 (2013).

[35]E. R. Johnson, A. Otero de la Roza, and S. G. Dale, J. Chem. Phys. **139**, 184116 (2013).

[36]A. D. Becke, J. Chem. Phys. **140**, 18A301 (2014).

[37]A. D. Becke, Phys. Rev. A **38**, 3098 (1988).

[38]H. Iikura, T. Tsuneda, T. Yanai, and K. Hirao, J. Chem. Phys. **115**, 3540 (2001).

[39]A. Becke and M. Roussel, Phys. Rev. A **39**, 3761 (1989).

[40]E. I. Sánchez-Flores, R. Chávez-Calvillo, T. A. Keith, G. Cuevas, T. Rocha-Rinza, and F. Cortés-Guzmán, J. Comp. Chem. **35**, 820 (2014).

[41]R. Bauernschmitt and R. Ahlrichs, .

[42]M. E. Casida and T. A. Wesolowski, Int. J. Quantum Chem. **96**, 577 (2004).

[43]A. D. Becke and E. R. Johnson, J. Chem. Phys. **123**, 154101 (2005).

[44]The postg program can be downloaded from `http://schooner.chem.dal.ca`.

[45]F. L. Hirshfeld, Theor. Chim. Acta **44**, 129 (1977).

[46]T. Han, Y. Hong, N. Xie, S. Chen, N. Zhao, E. Zhao, J. W. Y. Lam, H. H. Y. Sung, Y. Dong, B. Tong, and B. Z. Tang, J. Mater. Chem. C **1**, 7314 (2013).

[47]F. H. Allen, Acta Cryst. B **58**, 380 (2002), crystal structures can be obtained free of charge via http://www.ccdc.cam.ac.uk/data_request/cif.

[48]A. Becke, J. Chem. Phys. **85**, 7184 (1986).

[49]J. P. Perdew, K. Burke, and M. Ernzerhof, Phys. Rev. Lett. **77**, 3865 (1996).

[50]A. Otero-de-la Roza and E. R. Johnson, J. Chem. Phys. **136**, 174109 (2012).

[51]P. Giannozzi, S. Baroni, N. Bonini, M. Calandra, R. Car, C. Cavazzoni, D. Ceresoli, G. Chiarotti, M. Cococcioni, I. Dabo, *et al.*, J. Phys.: Condens. Matter **21**, 395502 (2009).

[52]A. Otero-de-la Roza, E. R. Johnson, and V. Luaña, Comput. Phys. Commun. **185**, 1007 (2014).

[53]A. Dreuw and M. Head-Gordon, J. Am. Chem. Soc. **126**, 4007 (2004).

[54]M. J. G. Peach, P. Benfield, T. Helgaker, and D. J. Tozer, J. Chem. Phys. **128**, 044118 (2008).

[55]K. A. Nguyen, R. Ruth Pachter, and P. N. Day, J. Chem. Phys. **140**, 244101 (2014).

[56]A. D. Laurent and D. Jacquemin, Int. J. Quantum Chem. **113**, 2019 (2013).

[57]T. Koerzdoerfer, J. S. Sears, C. Sutton, and J. L. Bredas, J. Chem. Phys. **135**, 204107 (2011).

[58]S. R. Whittleton, X. A. S. Vazquez, C. M. Isborn, and E. R. Johnson, J. Chem. Phys. **142**, 184106 (2015).

[59]K. Garrett, X. A. Sosa Vazquez, S. B. Egri, J. Wilmer, L. E. Johnson, B. H. Robinson, and C. M. Isborn, J. Chem. Theory Comput **10**, 3821 (2014).

TABLE I: Changes in molecular C_6 coefficients for a single excited moiety (single molecule or charge-transfer dimer) and overall dispersion energies for interaction of the chromophore with surrounding molecules in the crystal.

Molecule	$\%\Delta C_6$	ΔE_{disp} (kcal/mol)
4-amino-4′-nitrobiphenyl	0.3	-0.16
A3MN	0.9	0.17
coumarin	1.9	0.18
6-aminocoumarin	2.8	0.14
benzene/hexafluorobenzene	7.8	-1.24
N,N-dimethylaniline/hexafluorobenzene	2.8	0.07
naphthalene/hexafluorobenzene	4.6	1.23
tetracyanoethylene/naphthalene	-0.3	0.39
chloranilic acid/pyrazine	-0.3	0.46
2,5-dimethylbenzoquinone/bis(hydroquinone)	24.4	1.02

FIG. 1: The constituents of conjugated-chain set of molecules.

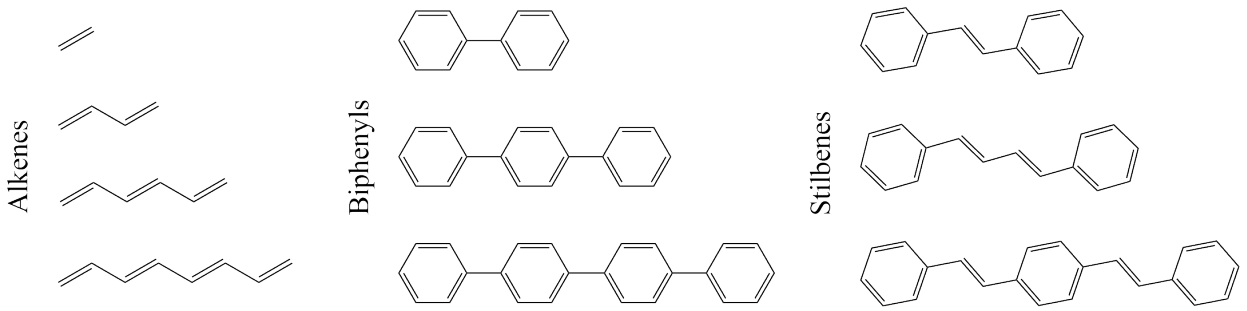

FIG. 2: Changes in molecular C_6 dispersion coefficients as a function of excitation energy for subsets of (a) alkenes and (b) stilbenes and biphenyls. Also shown are changes in C_6, C_8, and C_{10} dispersion coefficients for the conjugated-chain set as a function of chain length using two different definitions: (c) the Euclidean distance between terminal carbon atoms and (d) the number of C-C bonds forming the chain. The lines are to guide the eye.

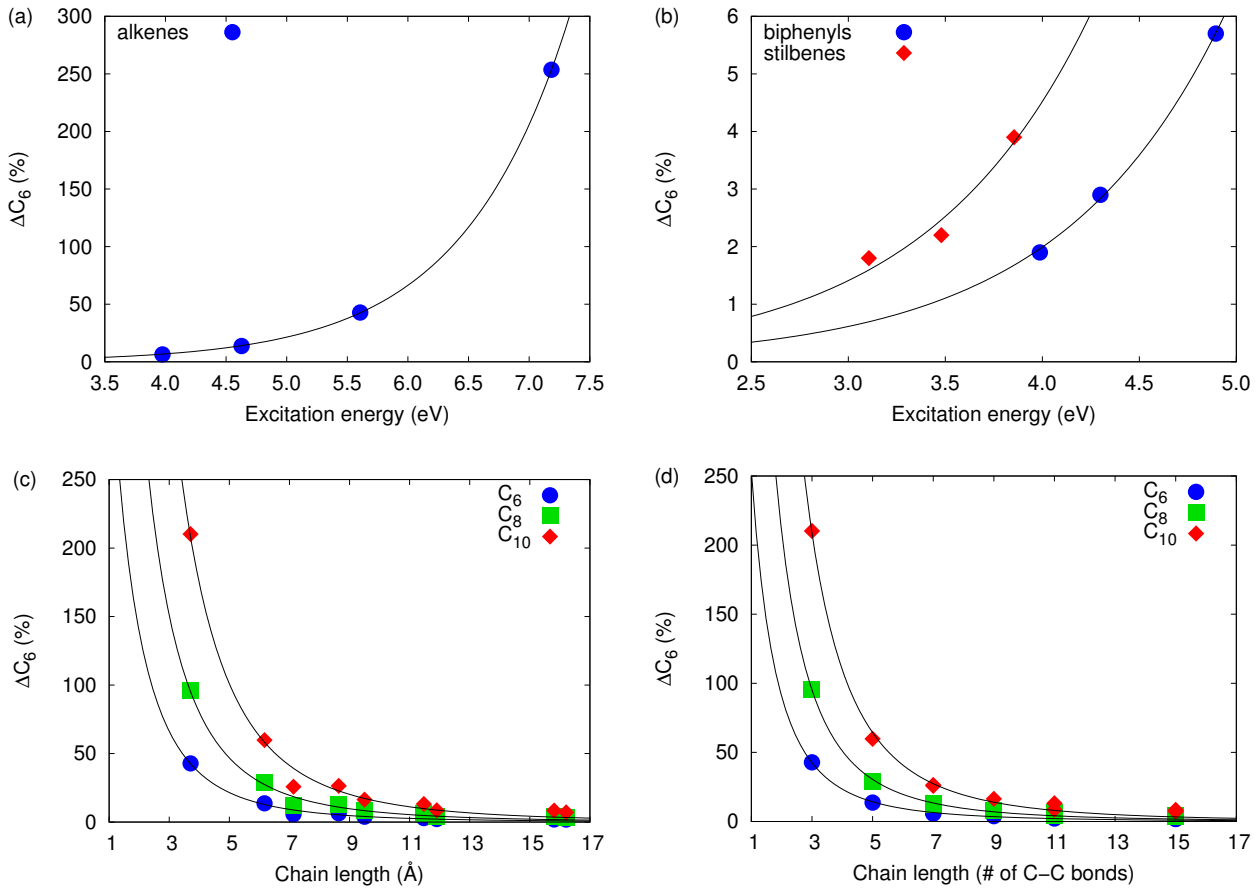

FIG. 3: Decomposition of the changes in molecular C_6 dispersion coefficients into contributions from the dipole-moment integrals and polarisabilities. Results are shown for the conjugated-chain set as a function of chain length, defined as the number of C-C bonds forming the chain.

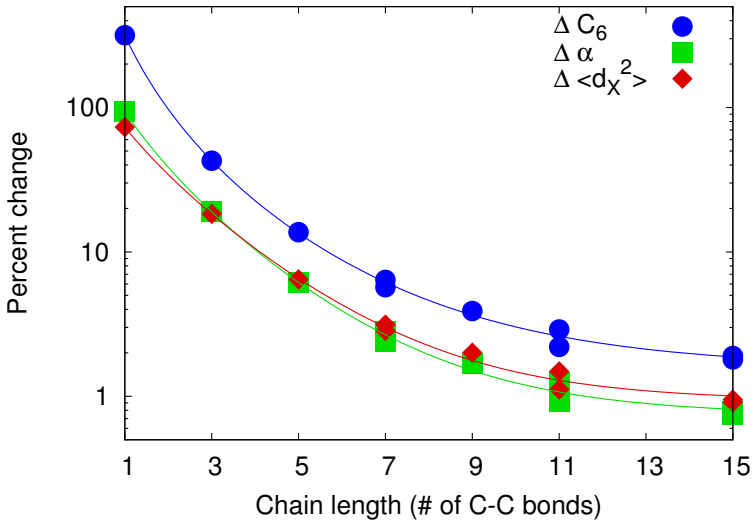

FIG. 4: The set of selected 4,4'-disubstituted biphenyls (a) together with the calculated extent of charge transfer as a function of excitation energy (b). Also shown are the excitation-induced changes in C_6 for the electron-donating and electron-withdrawing halves of each biphenyl from B3LYP (c) and CAM-B3LYP (d). Coloured symbols correspond to hydroxyl electron donors and open symbols correspond to amino electron donors.

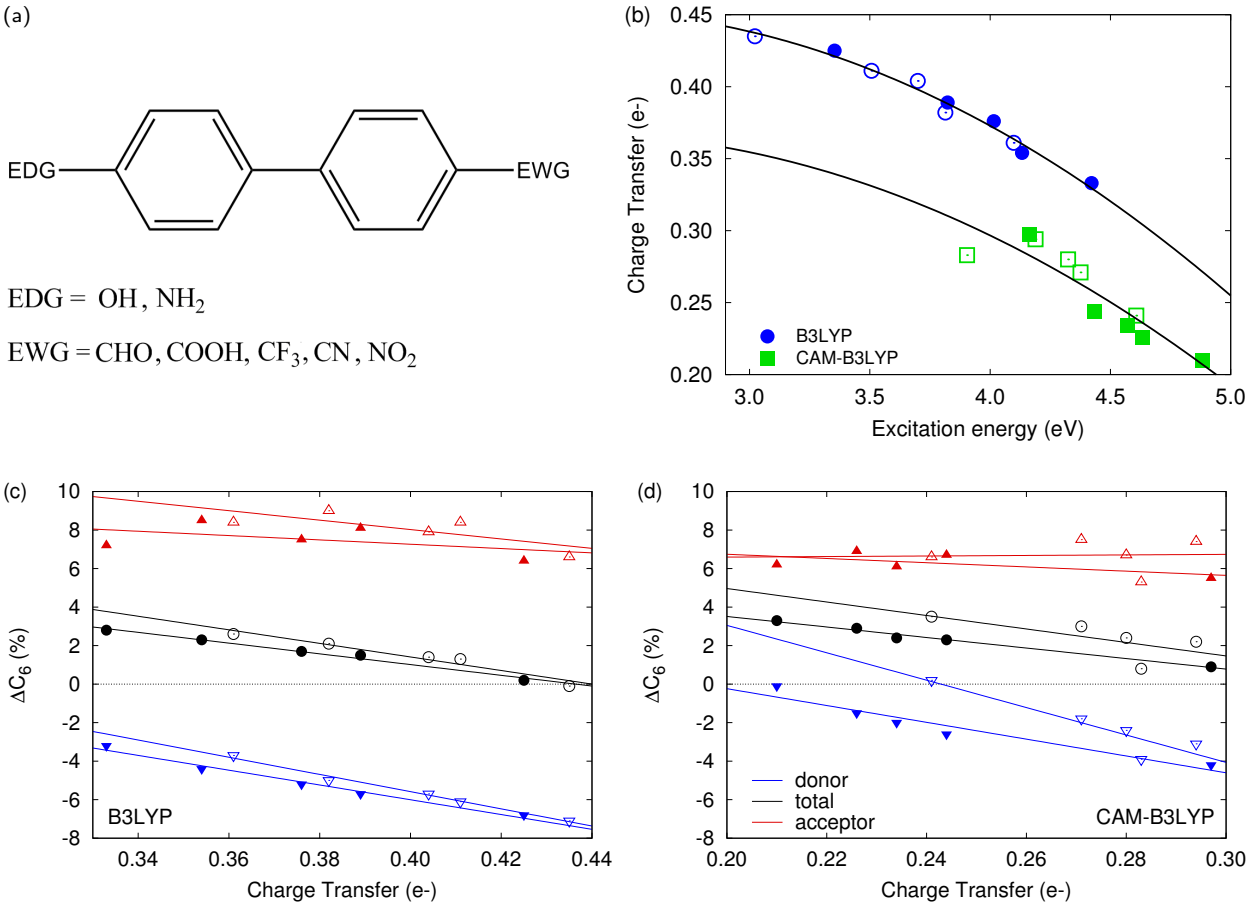

FIG. 5: Calculated properties of the benzene/hexafluorobenzene (left) and benzene/tetracyanoethylene (right) complexes as a function of exact-exchange mixing (a_X) in BLYP-based hybrids (filled symbols, solid lines) or range-separation (ω) parameters in LC-BLYP-based functionals (open symbols, dashed lines). Shown are the excitation energies (top row), extent of excitation-induced charge transfer (middle row), and excitation-induced changes in C_6 dispersion coefficients (bottom row).

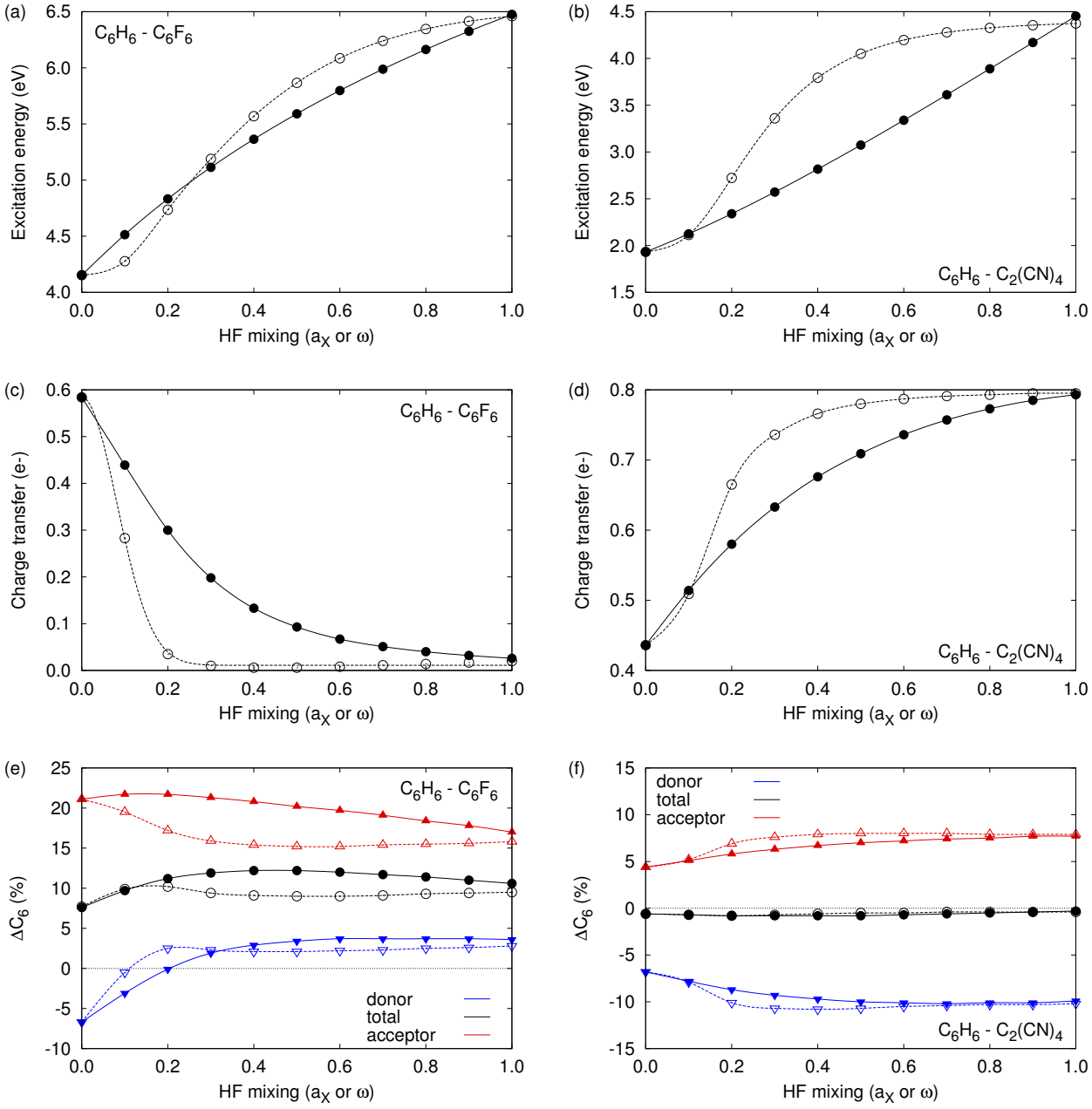

FIG. 6: Structures of selected chromophores present in molecular crystals together with their CCDC codes.